Available online at www.sciencedirect.com
SCIENCE DIRECT®
Journal of Magnetic Resonance 175 (2005) 210–221
JMR Journal of Magnetic Resonance
www.elsevier.com/locate/jmr

A ^{13}C field-cycling NMR relaxometry investigation of proton tunnelling in the hydrogen bond: Dynamic isotope effects, the influence of heteronuclear interactions and coupled relaxation

W. Wu, D.L. Noble, J.R. Owers-Bradley, A.J. Horsewill *

School of Physics and Astronomy, University of Nottingham, Nottingham NG7 2RD, UK

Received 21 January 2005; revised 6 April 2005
Available online 23 May 2005

Abstract

Concerted double proton transfer in the hydrogen bonds of a carboxylic acid dimer has been studied using ^{13}C field-cycling NMR relaxometry. Heteronuclear ^{13}C–^{1}H dipolar interactions dominate the ^{13}C spin–lattice relaxation which is significantly influenced by the polarisation state of the ^{1}H Zeeman reservoir. The methodology of field-cycling experiments for such heteronuclear spin-coupled systems is studied experimentally and theoretically, including an investigation of various saturation-recovery and polarisation-recovery pulse sequence schemes. A theoretical model of the spin–lattice relaxation of this coupled system is presented which is corroborated by experiment. Spectral density components with frequencies ω_C, $\omega_C + \omega_H$, and $\omega_C - \omega_H$ are mapped out experimentally from the magnetic field dependence of the ^{13}C and ^{1}H spin–lattice relaxation and the proton transfer rate at low temperature is determined from their widths. Any dynamic isotope effect on the proton tunnelling in the hydrogen bond arising from ^{13}C enrichment in the skeletal framework of the dimer is found to be smaller than experimental uncertainties (approximately 5%).

Keywords: Field cycling NMR relaxometry; Proton transfer; Proton tunnelling in the hydrogen bond; Heteronuclear relaxation; ^{13}C spin–lattice relaxation

1. Introduction

Spin–lattice relaxation has long been established as an effective and sensitive probe of molecular dynamics. The majority of investigations are conducted at constant magnetic field, monitoring changes in the relaxation efficiency as a function of temperature. However, with the advent of commercial magnetic field-cycling instruments there are an increasing number of research groups who are exploiting the benefits of studying the relaxation as a function of magnetic field and frequency. Unlike constant field measurements which sample the spectral density at a fixed frequency, field-cycling experiments are able to plot out the spectral density function directly [1–3].

In the solid state, particularly for systems exhibiting the motion of ^{1}H nuclei, it is common for the dominant relaxation mechanism to arise from the modulation of inter-nuclear dipolar interactions resulting from the relative motion of the nuclei as they are carried along with the molecular motion. Invariably this is modelled as a homonuclear interaction leading to terms which sample the spectral density at one and two times the Larmor frequency of the nucleus being investigated [4–6]. However, when multiple magnetic nuclei are present in the sample, heteronuclear dipolar interactions can provide relaxation pathways and the spectral density is sampled at sums and differences of the Larmor frequencies of the

* Corresponding author. Fax: +44 115 951 5180.
E-mail address: a.horsewill@nottingham.ac.uk (A.J. Horsewill).

1090-7807/$ - see front matter © 2005 Elsevier Inc. All rights reserved.
doi:10.1016/j.jmr.2005.04.003

participant nuclei [7]. Additionally, since two Zeeman reservoirs become coupled, the magnetisation recoveries of both sets of nuclei become bi-exponential.

In this paper, we have sought to explore the experimental consequences of heteronuclear dipolar interactions in spin–lattice relaxation, in particular with regard to field-cycling NMR relaxometry. The paper presents what we believe to be the first study of ^{13}C spin–lattice relaxation by field-cycling NMR. In conducting the investigation, there was a strong motivation to develop the techniques of field-cycling relaxometry and the methodology of data analysis for cases where heteronuclear dipolar interactions are present. Not only do many samples naturally contain multiple magnetic nuclei, but also this is relevant, for example, to the study of complex systems of biological interest where isotopic labelling and deuteration may be used to discriminate different functional sites. Furthermore, in our long-standing investigations of molecular tunnelling there is a motivation to study quantum isotope effects associated with isotopic substitution of the skeletal framework of a molecule. When light atoms move, there is a commensurate displacement of the heavy atoms of the molecular skeleton. Motion of the system along the tunnelling coordinate is in fact properly described as motion on a multi-dimensional potential energy surface (PES) and the quasi-particle contains admixtures of heavy atom displacements including, in our case, ^{13}C. This has the potential to illuminate our understanding of the coupling between small amplitude molecular vibrations and large amplitude atomic motion.

The system chosen for this investigation is one which is now very well characterised and understood, namely concerted double proton transfer in benzoic acid (BA), a carboxylic acid dimer, Fig. 1. There are two energetically non-equivalent tautomers labelled *L* and *R* with energy asymmetry *A*, which occupy potential wells in the PES landscape. They interchange by double proton transfer within the bridging hydrogen bonds of the dimer. The mechanism underlying the motion is dominated by phonon-assisted tunnelling and this is well established as the model system for translational molecular tunnelling [5,8–25]. We have made 99% ^{13}C substitution of the carboxy-carbon which now acts as a 'spy nucleus' monitoring the concerted motion of the two hydrogen atoms in the hydrogen bonds that bridge the BA dimer. In fact this arrangement represents a perceived advantage of studying heteronuclear relaxation since the system is very 'clean'; relaxation of the ^{13}C is dominated by just two symmetry related intra-dimer dipolar contacts with the two dynamic protons. There are no homonuclear ^{13}C interactions contributing to the relaxation, neither do inter-dimer heteronuclear interactions feature prominently. However, it will be shown that the polarisation state of the ^{1}H reservoir has a significant impact on the ^{13}C relaxation and the methodology of conducting a field-cycling experiment will be explored.

2. Theory

The ^{13}C enriched BA dimer contains two species of magnetic nuclei, ^{13}C and ^{1}H, both spin 1/2 and each possesses a thermal reservoir associated with its Zeeman energy. We shall use the symbols *I* and *S* to represent the ^{1}H and ^{13}C spin systems, respectively. Mutual

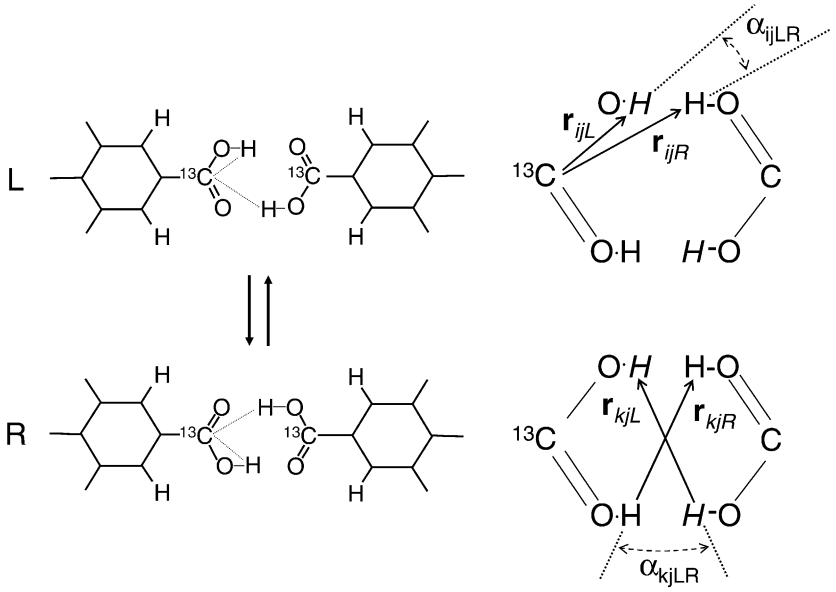

Fig. 1. The two tautomers of the BA dimer (labelled *L* and *R*). Some geometrical parameters that determine the dipolar interactions responsible for driving the spin–lattice relaxation are defined; these include heteronuclear (^{13}C–^{1}H) and homonuclear (^{1}H–^{1}H) dipolar contacts.

interactions between the two give rise to a coupling of the two reservoirs and their spin–lattice relaxation behaviour is therefore interdependent.

It is well established that spin–lattice relaxation in BA in the solid state is dominated by modulation of the inter-nuclear dipolar interactions arising from proton transfer in the bridging hydrogen bonds of the dimer. Expressions for the spin–lattice relaxation arising from both heteronuclear and homonuclear interactions with the protons in the hydrogen bond have been given in earlier papers for single crystal and powder samples [6,8,10,16,18,26,27]. The differential equations governing the longitudinal polarisations $\langle I_z\rangle$ and $\langle S_z\rangle$ are given by [7]

$$\begin{bmatrix} \frac{\mathrm{d}}{\mathrm{d}t}\langle I_z\rangle \\ \frac{\mathrm{d}}{\mathrm{d}t}\langle S_z\rangle \end{bmatrix} = -\begin{bmatrix} \rho_I & \sigma \\ \sigma & \rho_S \end{bmatrix}\begin{bmatrix} (\langle I_z\rangle - I_0) \\ (\langle S_z\rangle - S_0) \end{bmatrix}. \tag{1}$$

I_0 and S_0 are the polarisations of ^{1}H and ^{13}C, respectively, at thermal equilibrium. Longitudinal polarisation represents the population difference of the Zeeman levels, proportional to the respective magnetogyric ratio γ_H or γ_C. This is to be distinguished from the magnetisation measured in an NMR experiment which, although also a measure of population difference, is proportional to γ^2. The phrase 'magnetisation' will be used to refer to the signal measured in an NMR experiment, however, in computing the recovery curves $\langle I_z(t)\rangle$ and $\langle S_z(t)\rangle$ it is the polarisation which is the relevant quantity.

The elements of the relaxation matrix,

$$\mathbf{R} = \begin{pmatrix} \rho_I & \sigma \\ \sigma & \rho_S \end{pmatrix},$$

are inverse spin–lattice relaxation times defined in terms of spectral density contributions sampled at the Larmor frequencies of the ^{1}H and ^{13}C spins (ω_H and ω_C, respectively) and sums and differences of the two. For heteronuclear interactions in a powder sample, the elements of $\mathbf{R}$ have the form [7]:

$$\begin{aligned}
\rho_I^{CH} &= C_{CH}\frac{4a}{(1+a)^2}(L(\omega_H-\omega_C,\tau_c)+3L(\omega_H,\tau_c)\\
&\quad +6L(\omega_H+\omega_C,\tau_c)),\\
\sigma^{CH} &= C_{CH}\frac{4a}{(1+a)^2}(-L(\omega_H-\omega_C,\tau_c)\\
&\quad +6L(\omega_H+\omega_C,\tau_c)),\\
\rho_S^{CH} &= C_{CH}\frac{4a}{(1+a)^2}(L(\omega_C-\omega_H,\tau_c)+3L(\omega_C,\tau_c)\\
&\quad +6L(\omega_C+\omega_H,\tau_c)).
\end{aligned} \tag{2}$$

Here, $L(\omega,\tau_c)=\tau_c/(1+\omega^2\tau_c^2)$ is a Lorentzian with half-width at half-maximum amplitude equal to the inverse correlation time τ_c^{-1} and $a=\exp(A/k_BT)$ where A is the energy asymmetry of the two tautomeric forms L and R. C_{CH} is a lattice sum of dipolar interactions,

$$C_{CH} = \frac{\gamma_H^2\gamma_C^2\hbar^2}{40}\left(\frac{\mu_0}{4\pi}\right)^2 \times \sum_{i,j}\left[r_{ijL}^{-6}+r_{ijR}^{-6}+r_{ijL}^{-3}r_{ijR}^{-3}(1-3\cos^2\alpha_{ijLR})\right]. \tag{3}$$

The sum involves ^{13}C nuclei (labelled i) interacting with the ^{1}H nuclei (labelled j) which undergo proton transfer. The geometrical parameters are defined in Fig. 1.

Homonuclear ^{1}H–^{1}H interactions also contribute to ρ_I and for a powder sample,

$$\rho_I^{HH} = C_{HH}\frac{4a}{(1+a)^2}(L(\omega_H,\tau_c)+4L(2\omega_H,\tau_c)), \tag{4}$$

where

$$C_{HH} = \frac{3\gamma_H^4\hbar^2}{40}\left(\frac{\mu_0}{4\pi}\right)^2 \times \sum_{k,j}\left[r_{kjL}^{-6}+r_{kjR}^{-6}+r_{kjL}^{-3}r_{kjR}^{-3}(1-3\cos^2\alpha_{kjLR})\right]\frac{1}{N}, \tag{5}$$

which is a lattice sum involving the dipolar contacts of all protons (labelled k), including those on the phenyl ring, with the hydrogen bond protons (labelled j) which undergo proton transfer. $N=6$ is the number of protons in the BA molecule.

In deriving Eqs. (2) and (4) from the spectral density functions, it is assumed that the proton dynamics are stochastic hops and therefore the correlation functions are exponential decays. That this is so for concerted double proton transfer in carboxylic acids in general, and in BA in particular, has been established experimentally to a high degree of precision in previous field-cycling investigations [10,12,15,16].

Summing heteronuclear and homonuclear contributions, the overall relaxation may now be characterised by the matrix,

$$\mathbf{R} = \begin{pmatrix} \rho_I & \sigma \\ \sigma & \rho_S \end{pmatrix} = \begin{pmatrix} \rho_I^{CH} & \sigma^{CH} \\ \sigma^{CH} & \rho_S^{CH} \end{pmatrix} + \begin{pmatrix} \rho_I^{HH} & 0 \\ 0 & 0 \end{pmatrix}. \tag{6}$$

The general solutions of (1) describing the polarisation recovery following a disturbance away from equilibrium are a weighted sum of two exponentials:

$$\begin{aligned}
\langle I_z\rangle &= I_0(c_1^I\exp(-R_1t)+c_2^I\exp(-R_2t))+I_0,\\
\langle S_z\rangle &= S_0(c_1^S\exp(-R_1t)+c_2^S\exp(-R_2t))+S_0,
\end{aligned} \tag{7}$$

where the weighting coefficients c are functions of R_1, R_2, and $\mathbf{R}$, determined by the polarisation state of each reservoir at time $t=0$. The spin–lattice relaxation rates R_1 and R_2 are eigenvalues of $\mathbf{R}$, namely,

$$R_{1,2} = \tfrac{1}{2}((\rho_I+\rho_S)\pm\sqrt{(\rho_I-\rho_S)^2+4\sigma^2}). \tag{8}$$

The foregoing analysis highlights two consequences for the spin–lattice relaxation of both ^{13}C and ^{1}H species:

(a) the spectral density is sampled at multiple frequencies, (b) in general, the magnetisation recovery curves will be bi-exponential.

We can determine analytical expressions for the weighting coefficients under certain idealised initial conditions for the polarisation states of the two spin species. In an experiment in which the ^{13}C nuclei are irradiated but the ^{1}H are not, a conventional saturation-recovery sequence would prepare the system in the initial state, $\langle S_z\rangle_{t=0} = 0$, $\langle I_z\rangle_{t=0} = I_0$; in this case, we find the weighting coefficients characterising the ^{13}C polarisation recovery to be

$$c_1^S = \frac{(\rho_S - R_2)}{(R_2 - R_1)} \quad \text{and} \quad c_2^S = -1 - c_1^S. \tag{9}$$

Similarly in a saturation-recovery experiment on ^{1}H which establishes the initial conditions, $\langle I_z\rangle_{t=0} = 0$, $\langle S_z\rangle_{t=0} = S_0$, then the weighting coefficients characterising the ^{1}H polarisation recovery are

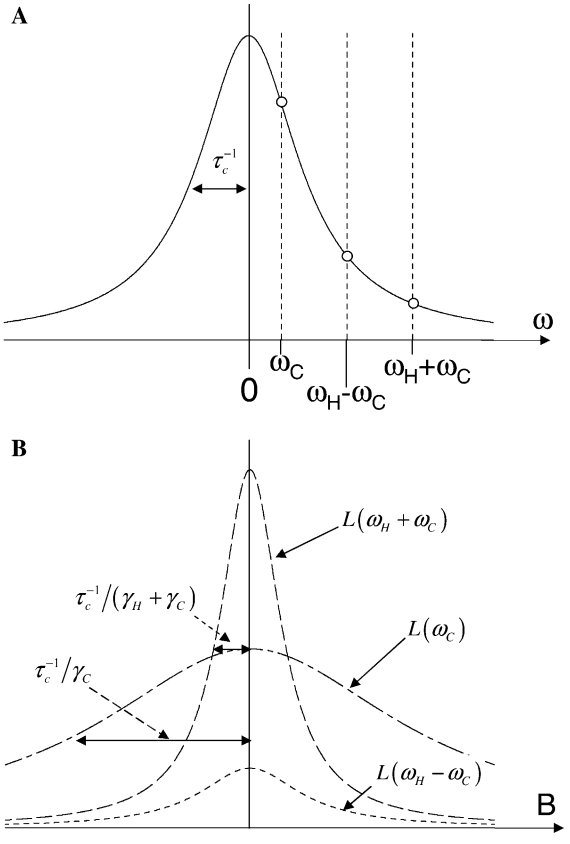

Fig. 2. Two outlooks on the spectral density function: (A) plotted as a function of frequency, ω, where the half-width at half-maximum is equal to the correlation rate, τ_c^{-1}. In a spin–lattice relaxation experiment, this curve is sampled at the three frequencies ω_C, $\omega_H + \omega_C$, and $\omega_H - \omega_C$, (B) plotted as a function of B-field, as applicable to field-cycling NMR. The proton transfer dynamics are determined by τ_c^{-1} but the observed spin–lattice relaxation is determined by the sum of three Lorentzian components with widths τ_c^{-1}/γ_C, $\tau_c^{-1}/(\gamma_H + \gamma_C)$, and $\tau_c^{-1}/(\gamma_H - \gamma_C)$.

$$c_1^I = \frac{(\rho_I - R_2)}{(R_2 - R_1)} \quad \text{and} \quad c_2^I = -1 - c_1^I. \tag{10}$$

2.1. Implications for field-cycling relaxometry

The spin–lattice relaxation rate constants are weighted sums of various Lorentzian lineshapes, Eqs. (2) and (4). There are two outlooks on an experiment to study molecular dynamics by NMR relaxometry. In the first, plotting T_1^{-1} as a function of frequency, Fig. 2A, the width of the spectral density curve is determined by τ_c^{-1} and the experiment samples this function at the specified frequencies. In the second, relevant to a field-cycling study of spin–lattice relaxation, plotting T_1^{-1} as a function of magnetic field, Fig. 2B, the observed relaxation is a sum of Lorentzians with different width. Therefore, it is to be expected that, in interpreting such experimental data, information on the amplitudes of the various Lorentzian components would be required to unambiguously determine an accurate value for the correlation rate.

Additionally, the spin–lattice relaxation rate constants R_1 and R_2 are molecular properties, independent of the experimental procedures, but the weighting coefficients, c, depend on the initial polarisation states of both Zeeman reservoirs. Therefore, to obtain magnetisation recovery curves from which molecular parameters can be reliably recovered, the preparation of the initial states need to be rigorously systematic. This may need special procedures in the case of field-cycling relaxometry. We shall return to a discussion of these issues in the light of experimental data.

3. Experimental details

The custom built field-cycling NMR spectrometer has been described elsewhere [3]. The magnetic field was provided by a superconducting solenoid with low inductance (0.023 henry) and at the maximum operating current of 150 A, the B-field at the sample was 2.5 T. The B-field was accurately proportional to the instantaneous current and the maximum field-switching rate was 10 T s^{-1}, although a rate of 8 T s^{-1} was routinely employed in most experiments. The Apollo digital NMR console was supplied by Tecmag and the control signals defining the magnetic field were derived from a 'gradient field' controller supplied with the instrument. The field cycling profiles were therefore straightforwardly integrated into the NMR pulse sequence using the software provided with this instrument. Automation was achieved using a Visual Basic script.

A variety of pulse sequences were employed to study the spin–lattice relaxation. These are described in Sections 4.2 and 5.2, Fig. 5. In all cases, saturation was achieved using a comb of six $\pi/2$ pulses and the

longitudinal polarisation of the nucleus of interest was measured with a single pulse. Using logarithmic increments in τ, magnetisation recovery curves were recorded from which the spin–lattice relaxation parameters were obtained.

The enriched (99 atom %) [*carboxy*-^{13}C]benzoic acid ($C_6H_5{}^{13}COOH$) was obtained commercially and used without further purification. The sample temperature was controlled by a variable flow helium cryostat that was incorporated into the cryostat of the superconducting magnet (supplied by Cryogenic Ltd). Sample temperatures in the range 4–300 K were measured with a calibrated Cernox resistance thermometer; the long-term stability and accuracy of the temperature in the region 20 K was better than 0.01 K.

4. Results and discussion

4.1. ^{13}C and ^{1}H spin–lattice relaxation at constant field

^{13}C and ^{1}H magnetisation recovery curves were recorded as a function of temperature using a saturation-recovery pulse sequence at fixed magnetic field, 0.8878 T (37.8 MHz) for ^{1}H and 2.428 T (26 MHz) for ^{13}C. In these experiments, at time $t = 0$, the magnetisation of the nuclear species under investigation was saturated while the polarisation of the second nuclear species was established close to its thermal equilibrium value (i.e., for ^{13}C: $\langle S_z\rangle_{t=0} = 0$, $\langle I_z\rangle_{t=0} = I_0$ and for ^{1}H: $\langle S_z\rangle_{t=0} = S_0$, $\langle I_z\rangle_{t=0} = 0$). The magnetisation recovery curves for both nuclei were well represented by a single exponential with a single time constant, $T_1^{(\mathrm{eff})}$, within experimental error. The relaxation time data are plotted in Fig. 3 as a function of inverse temperature.

That the magnetisation recovery for both nuclei is single exponential is a significant observation. This suggests that the off-diagonal elements of the relaxation matrix, σ, are small by comparison with the diagonal terms ρ_I and ρ_S. Simulations also show that the effects of the off-diagonal terms are further minimised by preparing the polarisation of the 'second' nucleus close to its thermal equilibrium value, Eq. (1). This being the case, the two observed relaxation times $T_{1I}^{(\mathrm{eff})}$ and $T_{1S}^{(\mathrm{eff})}$ should closely approximate ρ_I^{-1} and ρ_S^{-1}, respectively, under the measured conditions of magnetic field and temperature, Eq. (1). To assess the validity of this assertion, the values of the relaxation matrix have been calculated using the following procedure:

(i) *Determination of the dipolar relaxation constants:* the value of C_{CH} was calculated from Eq. (3) given the atomic coordinates determined at low temperature by single crystal neutron diffraction [20]. For this purpose, it was sufficient to include only intra-dimer contributions since, for ^{13}C–^{1}H interactions, these dominate over inter-dimer contributions. In performing this calculation, as in [15], the atomic coordinates of the energetically less favourable dimer were determined by rotating the dimer about its central axis. The calculated value is $C_{\mathrm{CH}}^{(\mathrm{calc})} = 1.36 \times 10^7\ \mathrm{s}^{-2}$. The value $C_{\mathrm{HH}} = 6.3 \times 10^7\ \mathrm{s}^{-2}$ was obtained from the field-cycling ^{1}H NMR relaxometry study of BA in natural isotopic abundance [16].

(ii) *Simulation of proton transfer rate:* for the purposes of analysing the temperature dependence data, the correlation rate, τ_c^{-1}, was modelled using the dynamical parameters determined in earlier investigations of proton transfer in benzoic acid [10,14,16]

$$\tau_c^{-1} = 1.22 \times 10^8 \coth\left(\frac{A}{k_B T}\right) + 1 \times 10^{10} \times \exp\left(\frac{-180}{T}\right) + 5 \times 10^{11} \exp\left(\frac{-600}{T}\right). \quad (11)$$

The first term on the right-hand side is a contribution from proton tunnelling in the ground state, the second term is due to tunnelling in an intermediate state and the final term is an Arrhenius law to accommodate the Boltzmann weighted average of through barrier processes via states higher up the barrier (pseudo-classical dynamics). The reader is referred to [9,14,16] for further details.

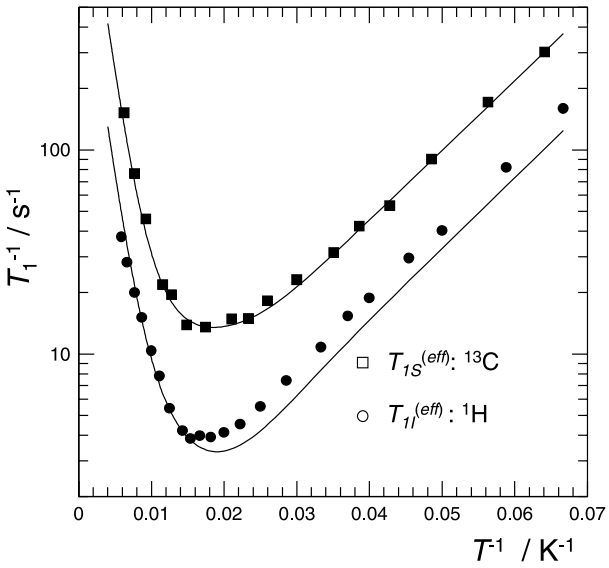

Fig. 3. The inverse temperature dependence of the effective ^{13}C and ^{1}H spin–lattice relaxation time parameters $T_{1S}^{(\mathrm{eff})}$ and $T_{1I}^{(\mathrm{eff})}$ recorded at constant field in each case. (^{13}C: 26 MHz, $B = 2.428$ T. ^{1}H: 37.8 MHz, $B = 0.8878$ T). The solid lines are calculated with dipolar constants $C_{\mathrm{CH}} = 1.36 \times 10^7\ \mathrm{s}^{-2}$ and $C_{\mathrm{HH}} = 6.3 \times 10^7\ \mathrm{s}^{-2}$.

In Fig. 4, the calculated values of the relaxation time constants R_1^{-1} and R_2^{-1} (dashed lines) and the weighting coefficients $c_2^{I,S}$ and $c_1^{I,S}$ are presented as a function of

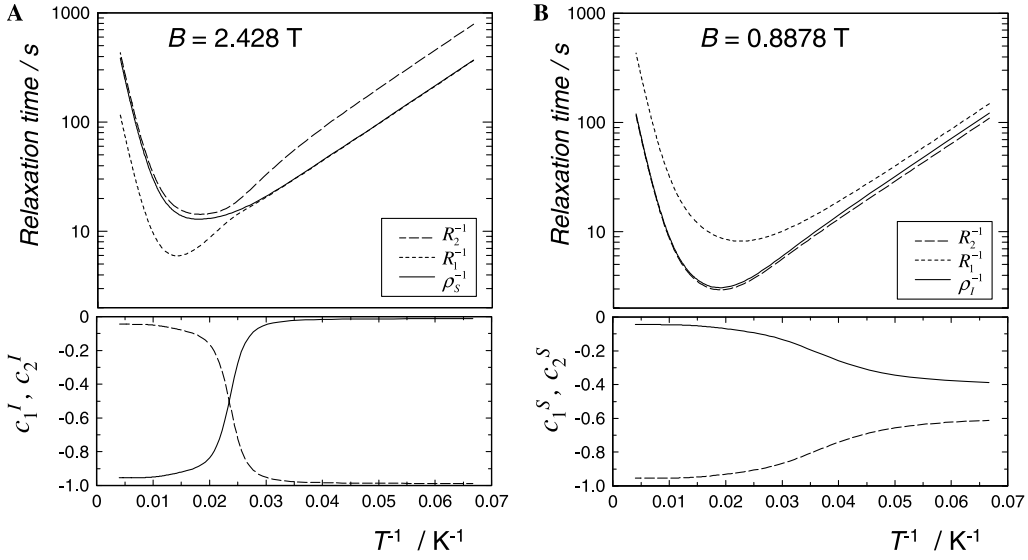

Fig. 4. Calculations as a function of inverse temperature of the relaxation time constants R_1^{-1} and R_2^{-1} (dashed lines) and the weighting coefficients $c_2^{I,S}$ (solid line) and $c_1^{I,S}$ (dashed line): (A) $B = 2.428$ T and (B) $B = 0.8878$ T. The weighted means of R_1^{-1} and R_2^{-1} correspond closely with the respective inverse diagonal elements of the relaxation matrix ρ_I^{-1} and ρ_S^{-1} (solid lines).

temperature for two values of magnetic field: (A) $B = 2.428$ T, appropriate to the ^{13}C saturation-recovery experiments, and (B) $B = 0.8878$ T, appropriate to the ^{1}H saturation-recovery experiments. Inspection of the calculated weighting coefficients shows that across a wide temperature range, the ^{13}C relaxation, Fig. 4A, is indeed dominated by one exponential component. Only in a narrow temperature region do the weighting coefficients adopt values significantly different from 0 and 1, however, in this region R_1 and R_2 have similar values, so it is doubtful that the observed magnetisation recovery will deviate significantly from a single exponential function. Therefore, the calculated behaviour shows that in practice the ^{13}C magnetisation recovery over the whole temperature range will be characterised by a single relaxation time constant, in agreement with observation. Similarly for the ^{1}H relaxation represented in Fig. 4B; there is bi-exponential character revealed in the values of the weighting coefficients at low temperature, but the values of R_1 and R_2 are insufficiently different for the ^{1}H relaxation to be distinguished from a single exponential.

To compare the calculated behaviour with the ^{13}C experiment, we equate the effective T_1 at $B = 2.428$ T with the weighted mean of the two spin–lattice relaxation time constants,

$$T_{1S}^{(\mathrm{eff})} = \frac{c_1^S/R_1 + c_2^S/R_2}{c_1^S + c_2^S}. \tag{12}$$

Similarly, using the same parameter set but at $B = 0.8878$ T we have evaluated the effective T_1 for the ^{1}H NMR constant field spin–lattice relaxation experiments,

$$T_{1I}^{(\mathrm{eff})} = \frac{c_1^I/R_1 + c_2^I/R_2}{c_1^I + c_2^I}. \tag{13}$$

These functions are plotted in Fig. 3 (solid lines) and reveal good agreement with both the ^{1}H and the ^{13}C experimental data. Neither values C_{CH} or C_{HH} reported in (i) above were adjusted in calculating these curves. The best fit value of the energy asymmetry, $A/k_{\mathrm{B}} = 80 \pm 2$ K, is consistent with the value reported for the sample with natural isotopic abundance [10,16].

It is notable and significant that the calculated values of $T_{1I}^{(\mathrm{eff})}$ and $T_{1S}^{(\mathrm{eff})}$ correspond very closely with the respective inverse diagonal elements ρ_I^{-1} and ρ_S^{-1} of the relaxation matrix; the latter are plotted in Fig. 4 (solid lines). This confirms the assertion made earlier and will facilitate the interpretation of the field-dependent T_1 data in later sections, including the extraction of accurate values of the correlation rate for proton transfer.

Concluding this section on the constant field experiments: using an estimate for the proton transfer correlation rate based on the behaviour of BA in natural isotopic abundance, Eq. (11), good agreement between the relaxation model and the experimental spin–lattice relaxation data is obtained. Clearly, the heteronuclear interactions play an important role in the relaxation processes. Indeed, it is the modulation of the ^{13}C–^{1}H interactions arising from the proton motion that drives the spin–lattice relaxation of the ^{13}C nuclei. However, for both nuclei the magnetisation recovery appears single exponential to within experimental error. This characteristic will be further explored in the context of variable field measurements in the next section.

4.2. Field cycling: ^{13}C and ^{1}H spin–lattice relaxation as a function of B-field

In a constant field experiment, it is relatively straightforward to prepare the system in a systematic state where, for example, one nuclear spin system is saturated while the second has its equilibrium polarisation. In a field-cycling experiment, where the nature of the experiment is such that the magnetic field is switched rapidly across a wide range of values this is less easy and it is evident that particular care must be taken to establish consistent polarisation states before each measurement.

First, we consider the results of a series of saturation-recovery experiments on ^{13}C. Three field-cycling sequences were employed as illustrated in Fig. 5, each designed to prepare the ^{1}H magnetisation differently.

Seq. A. Beginning from zero, the field was switched rapidly to the resonance condition for ^{13}C ($B_{^{13}C} = 2.026$ T, $\nu_{^{13}C} = 21.7$ MHz) where it remained for a period τ_S to create a pre-determined polarisation of the ^{1}H nuclei. The ^{13}C nuclei were then saturated with a burst of $\pi/2$ pulses before the field was rapidly switched to the field of interest, B_r, where the nuclei were allowed to relax for a time interval τ_r. A rapid field switch then took the field back to resonance with the ^{13}C nuclei and the ^{13}C magnetisation was measured with a $\pi/2$ pulse before the field reverted to zero.

Seq. B. In a variant to sequence *A*, a short pause at the resonance field of the ^{1}H nuclei ($B_{^{1}H} = 0.5092$ T, $\nu_{^{1}H} = 21.7$ MHz) was introduced into the field switch immediately following ^{13}C saturation; here, the ^{1}H nuclei were saturated with a burst of $\pi/2$ pulses.

Seq. C. In a third sequence, the sample was prepared at B_r for at least three times the proton T_1 before the ^{13}C magnetisation was saturated. This prepared the ^{1}H polarisation close to its thermal equilibrium value at the field the ^{13}C relaxation was to be recorded. It was expected that this experiment would minimise the effects of cross-relaxation between the two nuclear species.

4.2.1. Magnetisation recovery curves

Magnetisation recovery curves were recorded using the three field-cycling sequences. In Fig. 6, the

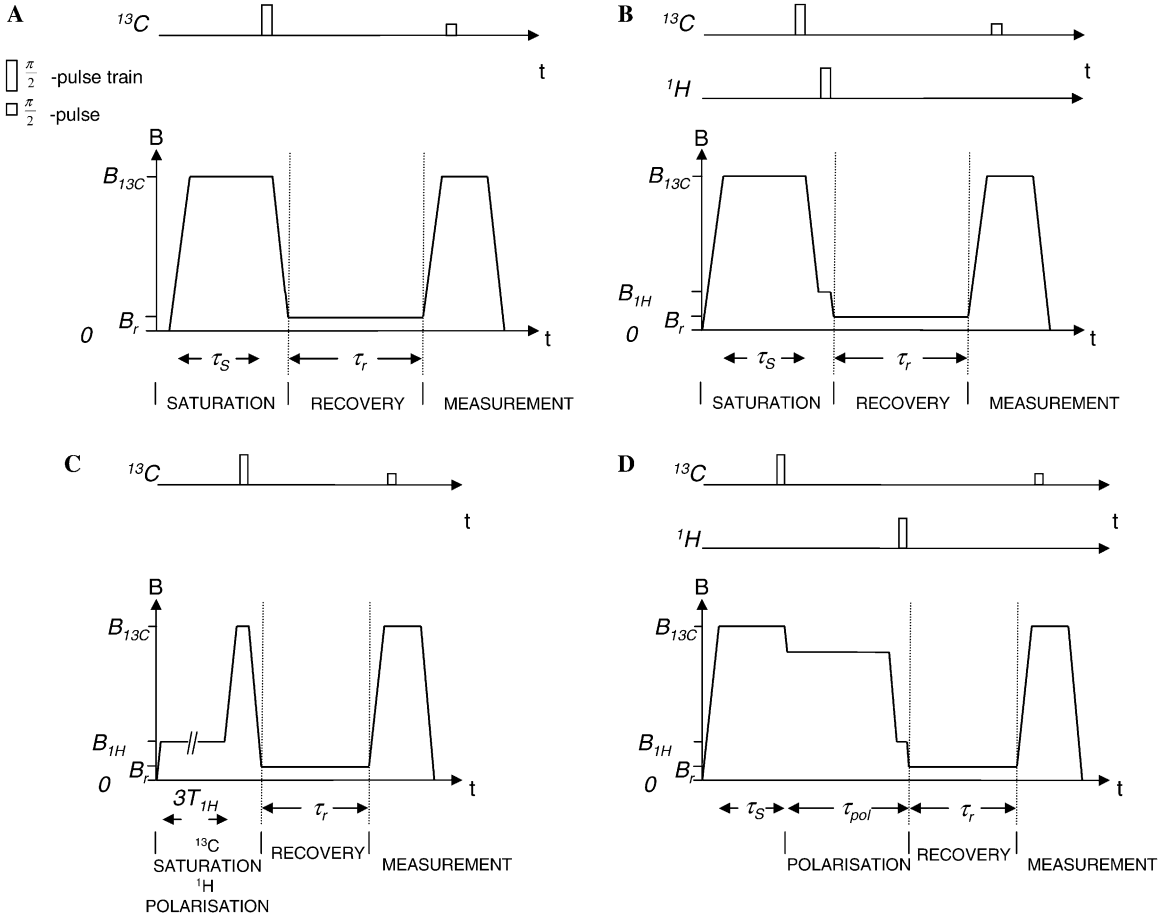

Fig. 5. The field-cycling pulse sequences used in this investigation. (A–C) Saturation-recovery experiments utilising different preparation regimes for the ^{1}H polarisation. (D) is a polarisation-recovery experiment. See text for details.

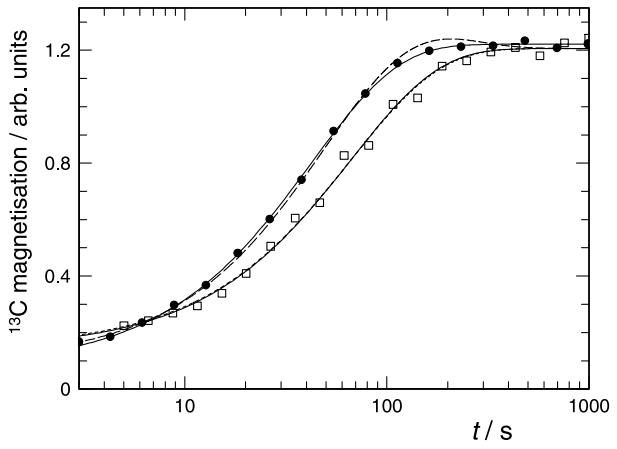

Fig. 6. ^{13}C magnetisation recovery curves recorded using saturation-recovery pulse sequences *A* (filled circles) and *C* (open squares): $B = 1.2$ T, $T = 20$ K. The simulations, representing the solutions of the coupled equations (1), are shown with dashed lines. The differences arise from the different initial polarisation states of the ^{1}H reservoir.

magnetisation recovery of ^{13}C arising from pulse sequences *A* and *C* is plotted; $B_r = 1.2$ T, $\tau_S = 10$ s, $T = 20$ K. A single exponential recovery law fitted well to each set of data and a relaxation time constant, $T_{1S}^{(\mathrm{eff})}$, was extracted. Within experimental uncertainties, no significant improvement was gained by fitting with a bi-exponential function. We observe a systematic difference between the two recovery curves leading to different $T_{1S}^{(\mathrm{eff})}$ values. As with constant field experiments, in no field-cycling experiment was it possible to definitively resolve two exponential components in any magnetisation recovery curve. The systematic differences arise from the preparation of the initial polarisation states and the resulting effects on the weighting coefficients, $c_{1,2}^S$.

We have simulated the solutions to Eq. (1) using the calculated relaxation matrix defined by the parameters $C_{\mathrm{CH}} = 1.36 \times 10^7\ \mathrm{s}^{-2}$ and $C_{\mathrm{HH}} = 6.3 \times 10^7\ \mathrm{s}^{-2}$ employed in the previous section. Computed ^{13}C magnetisation recoveries, subject to the initial conditions defined for sequences *A* and *C*, are superimposed on the experimental curves in Fig. 6 (dashed lines). In these calculations, we estimate that the initial proton polarisation for field cycling sequence *A* is approximately 10% of I_0 at 1 T. The model successfully simulates the apparent shortening of the effective T_1 when the initial proton polarisation differs from equilibrium. Close inspection of the simulation curve for sequence *A* reveals some bi-exponential character culminating in a very small nuclear Overhauser effect (NOE) enhancement of the ^{13}C polarisation during the approach to equilibrium. An NOE enhancement is not evident in this particular set of experimental data, but the predicted effect is not large compared with experimental uncertainties. Small NOE enhancements were observed in some experimental data sets. The agreement between the experimental and computed recovery curves is generally very good given: (i) the manner in which spin-diffusion is accommodated in the model, (ii) effects arising from relaxation during the field switches, and (iii) systematic uncertainties in our knowledge of the actual initial magnetisation states. The latter, may be a relevant issue, particularly for sequence *A*, since polarisation can be preserved for extended periods via the dipolar order, even if the field is switched to zero. An enhancement to Eq. (1) may indeed be required to incorporate such effects of dipolar order but, for the moment at least, to the level of approximation considered, this is beyond the scope of this present paper.

4.2.2. Magnetic field dependence: mapping the spectral density

Using the three saturation-recovery field-cycling sequences, the magnetic field dependence of the ^{13}C spin–lattice relaxation time, $T_{1S}^{(\mathrm{eff})}$, was measured at 20 K in the field range $0.4 \leqslant B_r \leqslant 2.3$ T. Measurements at fields lower than 0.4 T were impractical due to the small ^{13}C signal amplitude. The results are plotted in Fig. 7 as $(T_{1S}^{(\mathrm{eff})})^{-1}$ vs. B_r on log–log axes. Systematic differences in the measured values of $T_{1S}^{(\mathrm{eff})}$ of the kind illustrated in Fig. 6 are reflected in this graph. The band encompassing the three sets of data has a range of order 40%. However, significantly, the three curves are parallel to each other meaning that the information content regarding the proton transfer correlation rate is identical for the three sequences. Free-fits to the three relaxation curves separately provide correlation rates that agree to within 5%.

For sequences *A* and *B*, since the proton polarisation is far removed from equilibrium, the effects of cross-

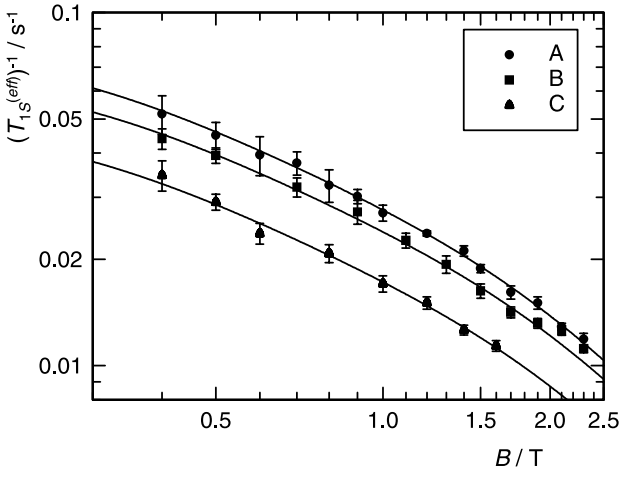

Fig. 7. The magnetic field dependence of the ^{13}C inverse spin–lattice relaxation time, $(T_{1S}^{(\mathrm{eff})})^{-1}$, recorded at $T = 20$ K using pulse sequences *A*, *B*, and *C*. The solid lines represent free-fits to Eq. (15). The initial ^{1}H polarisation states are different for the three sets of data but the curves are parallel indicating that the information content regarding the correlation rate, τ_c^{-1}, is same for all three.

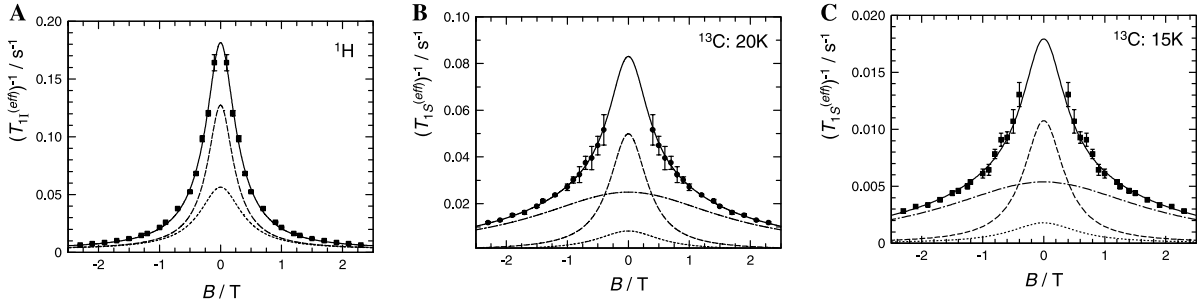

Fig. 8. The magnetic field dependence of the inverse spin–lattice relaxation times (A) ^{1}H: $T_{1I}^{(\mathrm{eff})}$ ($T = 20$ K), (B) ^{13}C: $T_{1S}^{(\mathrm{eff})}$ ($T = 20$ K), and (C) ^{13}C: $T_{1S}^{(\mathrm{eff})}$ ($T = 15$ K) where the proton transfer dynamics are dominated by phonon-assisted tunnelling. The data have been reflected in the B-axis to emphasise the Lorentzian character. Solid lines are fits to Eqs. (14) and (15), respectively. The dashed lines in (A) represent the heteronuclear (ρ_I^{CH}; long dash) and homonuclear (ρ_I^{HH}; short dash) components of Eq. (14). The dashed lines in (B) and (C) represent the three Lorentzian components of Eq. (15) ($L(\omega_{\mathrm{H}} + \omega_{\mathrm{C}})$, long dash; $L(\omega_{\mathrm{C}})$, dash-dot; $L(\omega_{\mathrm{H}} - \omega_{\mathrm{C}})$, short dash).

relaxation and the off-diagonal elements of the relaxation matrix influence the measured relaxation rates. Only for sequence C is cross-relaxation minimised. The disadvantage of this sequence, however, is the preparation time required. Since each data point on the magnetisation curve requires establishment of thermal equilibrium within the proton Zeeman reservoir, given the very long T_1 values, the measurement of a ^{13}C T_1 can become excessively time consuming, especially if full-field dependence is required. Fortunately, as is evident from the fits to the experimental data in Fig. 7 and the simulations, where the off-diagonal elements of **R** are small then to a good approximation only the amplitude and not the shape of the $T_{1S}^{(\mathrm{eff})}$ vs. B curve is affected by the preparation of the ^{1}H Zeeman reservoir.

The field dependence of the effective ^{1}H spin–lattice relaxation rate $(T_{1I}^{(\mathrm{eff})})^{-1}$ was also measured using field-cycling sequence A. These measurements were found to be independent of the initial polarisation state of the ^{13}C spins, consistent with the small heat capacity of the ^{13}C Zeeman reservoir. The ^{1}H data are plotted in Fig. 8A together with the ^{13}C data recorded using sequence a at two temperatures, 20 and 15 K (Figs. 8B and C, respectively). The data are plotted with log-linear axes and are reflected about the $B = 0$ axis to emphasise the Lorentzian lineshapes. It is noticeable that the width of the relaxation peak appears broader for the ^{13}C data than the ^{1}H data; this reflects not a difference in correlation rate but a difference in the frequencies at which the spectral density is sampled.

5. Discussion

5.1. Interpretation of the spectral densities

The experimental data in Fig. 8 represent a weighted mean of the spin–lattice relaxation rates R_1 and R_2, Eqs. (8), (12), and (13). Our objective is to interpret these data in terms of the various Lorentzian components that constitute the relaxation matrix and to extract the correlation time for proton transfer. Our approach will be necessarily pragmatic. Independent experimental information on the elements of **R** are unavailable to us, although the agreement with the temperature dependence data, the simulations of magnetisation recovery, and our knowledge of the proton transfer behaviour in samples with natural isotopic abundance, give us confidence that these can be calculated reliably in this particular material. Calculations confirm that at low temperature the values of $(T_{1I}^{(\mathrm{eff})})^{-1}$ and $(T_{1S}^{(\mathrm{eff})})^{-1}$ closely match the diagonal elements of **R**, ρ_I, and ρ_S, consistent with the off-diagonal elements being small. This being the case we are able to write:

$$\begin{aligned}(T_{1I}^{(\mathrm{eff})}(B))^{-1} &= \rho_I^{\mathrm{CH}} + \rho_I^{\mathrm{HH}} \\ &= K_{\mathrm{CH}}(L((\gamma_{\mathrm{H}} - \gamma_{\mathrm{C}})B, \tau_{\mathrm{c}}) \\ &\quad + 3L(\gamma_{\mathrm{H}}B, \tau_{\mathrm{c}}) + 6L((\gamma_{\mathrm{H}} + \gamma_{\mathrm{C}})B, \tau_{\mathrm{c}})) \\ &\quad + K_{\mathrm{HH}}(L(\gamma_{\mathrm{H}}B, \tau_{\mathrm{c}}) + 4L(2\gamma_{\mathrm{H}}B, \tau_{\mathrm{c}})) \qquad (14)\end{aligned}$$

and

$$\begin{aligned}(T_{1S}^{(\mathrm{eff})}(B))^{-1} &= \rho_S^{\mathrm{CH}} \\ &= K_{\mathrm{CH}}(L((\gamma_{\mathrm{C}} - \gamma_{\mathrm{H}})B, \tau_{\mathrm{c}}) \\ &\quad + 3L(\gamma_{\mathrm{C}}B, \tau_{\mathrm{c}}) + 6L((\gamma_{\mathrm{C}} + \gamma_{\mathrm{H}})B, \tau_{\mathrm{c}})), \qquad (15)\end{aligned}$$

where the functions are expressed in terms of the magnetic field B. The K's are the dipolar constants incorporating the temperature dependence factor associated with the energy asymmetry (see Eqs. (2) and (4)).

We have independently fitted the functions (14) and (15) above to the ^{1}H and ^{13}C T_1 data in Fig. 8, respectively, and the best fits are shown as solid lines; good agreement is observed. The dashed line curves depict the different Lorentzian components comprising the net spectral density. The proton transfer correlation rate values determined from the ^{13}C and ^{1}H data sets, $\tau_{\mathrm{c}}^{-1} = 1.24 \pm 0.04$ s^{-1} (^{13}C : 20 K), $\tau_{\mathrm{c}}^{-1} = 1.33 \pm 0.08$ s^{-1} (^{13}C : 15 K), and 1.25 ± 0.05 s^{-1} (^{1}H: 20 K), agree within experimental uncertainties.

5.2. Polarisation-recovery experiments

At low field, in this case defined as $B_r < 0.4$ T, the ^{13}C NMR signal is too small to make possible saturation-recovery experiments to measure the ^{13}C relaxation. In such cases in homonuclear field-cycling relaxometry it is customary practise to employ polarisation-recovery pulse sequences to record the relaxation properties. We have investigated the ^{13}C magnetisation recovery in such experiments on this heteronuclear material. Here, the spin systems are first polarised at high field before the field is switched to the low relaxation field, B_r, where the return to thermal equilibrium of the spins is monitored. The polarisation-recovery pulse sequence is illustrated in Fig. 5D and two variants were employed: in a first experiment the initial states of both ^{1}H and ^{13}C spins were polarised, whereas in a second experiment the ^{1}H polarisation was destroyed with a resonant pulse during the switch from the polarisation field to the low relaxation field. The magnetisation-recovery curves for these two experiments are depicted in Fig. 9 where the relaxation field was $B_r = 0.3$ T and the polarisation field was $B_{pol} = 1.5$ T. There is a considerable systematic difference in the recovery curves, reflecting the different initial polarisation states. A single exponential function can be fitted satisfactorily to both recovery curves (solid lines) but clearly there is underlying a significant bi-exponential character. As earlier with the saturation-recovery experiments, we have simulated the solutions of the coupled relaxation equations (1) with $C_{CH} = 1.36 \times 10^7\ s^{-2}$ and $C_{HH} = 6.3 \times 10^7\ s^{-2}$. Simulated curves are superimposed on the experimental data in Fig. 9 (dashed lines) and there is good agreement.

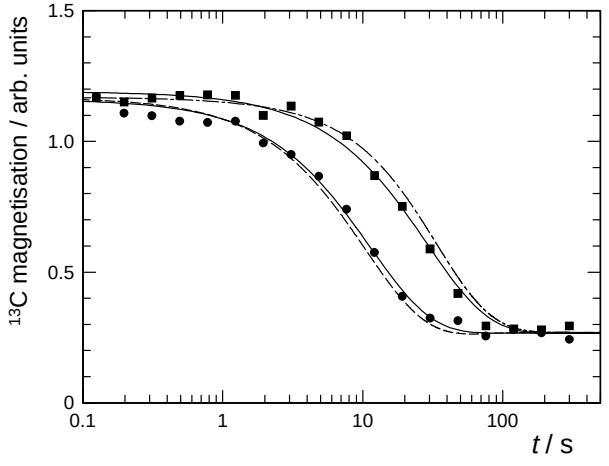

Fig. 9. ^{13}C magnetisation recovery curves recorded using polarisation-recovery pulse sequence *D* with and without initial polarisation of the ^{1}H reservoir. Filled circles, protons polarised. Filled circles, protons saturated. The simulations, representing the solutions of the coupled equations (1), are shown with dashed lines.

Clearly, the relaxation model is corroborated but where does this leave our experiment to measure the low field relaxation behaviour? It is difficult to see how such a polarisation-recovery experiment can independently lead to a measurement of a relaxation rate that can be plotted as a function of field to map out the spectral density. We are no longer in a regime where the effects of the off-diagonal elements of the relaxation matrix are negligible and where the observed relaxation rate corresponds closely with a diagonal element. Unless the ^{13}C signal-to-noise ratio is sufficiently good to facilitate an accurate bi-exponential analysis, no independent reduction of the polarisation-recovery data can lead to a relaxation rate that can be assimilated into the magnetic field dependent data of Figs. 7 and 8. Only if additional information from a model is input into the analysis can the polarisation-recovery curves be interpreted. Therefore, these polarisation-recovery data, together with the simulations, provide corroboration of the dynamical model for proton transfer and the relaxation model but it does not provide independent information on the correlation rate.

5.3. Effects of ^{13}C substitution on the proton transfer rate

At temperatures of 20 K and below, the proton transfer dynamics are dominated by ground state phonon-assisted tunnelling and the correlation rate is in the temperature-independent 'plateau' region [9,10,14,16]. We designate this as the 'tunnelling rate' and our experiments show that this value is the same within experimental error for ^{13}C-BA and BA in natural isotopic abundance [10,16]. Given the multi-dimensional character of the PES and the significant changes in bonding which occur as the protons move this result might be viewed as somewhat disappointing, especially as the tunnelling matrix element is an exponential function of the particle mass and the barrier properties. However, it is demonstrated how field-cycling experiments provide impressive accuracy (approximately 2% for homonuclear systems [10,16] and 5% for heteronuclear) in the determination of correlation rates and now that ab initio calculations of multi-dimensional tunnelling [28–31] are becoming tractable on systems of the size of BA it will provide a useful result against which to evaluate the theoretical framework and the efficacy of contemporary quantum chemistry computations.

6. Concluding remarks

Even though the ^{13}C abundance was enriched at the carboxyl site, the measurement of the ^{13}C relaxation properties was still a challenging one due to the small NMR signal amplitude arising from its small magnetogyric ratio and small mole fraction. Additionally, the

very long relaxation times often precluded the possibility of extensive signal averaging. Nonetheless, a very satisfactory account of the relaxation properties of a heteronuclear system has emerged from this investigation.

There is a sense in which the study of the ^{13}C relaxation in this material provides a very well-defined system with the ^{13}C nucleus acting as a 'spy' on the proton transfer dynamics; just two ^{13}C–^{1}H dipolar contacts dominate. The advantages are familiar in the guise of isotopic labelling but no spin system can act in isolation and the disadvantage is the additional complexity in the spectral density components. The study benefited from prior knowledge and experience of the BA system and the relaxation theory has been validated to a highly satisfactory degree of precision.

The relaxation theory for heteronuclear, coupled systems is long established but relatively few experimental investigations have been undertaken as a function of magnetic field. This study has confronted some interesting practical issues regarding the methodology of field-cycling relaxometry in heteronuclear spin systems. Clearly, the initial polarisation of the spin systems is an important factor and must not be overlooked as experiments on isotopically labelled samples become more prevalent, neither must spectral density components that characterise the heteronuclear interactions be ignored if accurate values of the correlation times are to emerge. Systematic effects influencing the interpretation of single-spin relaxation data are readily observable and must be accommodated in any model used to interpret the data. Furthermore, as strategies to enhance NMR signals from traditionally unreceptive systems via polarisation transfer become more prevalent, investigations such as this to quantify the coupling between spin reservoirs are likely to become more important.

The use of polarisation-recovery pulse sequences, often used in field-cycling, presents its own challenges for heteronuclear systems. Usually such schemes are necessary to obtain an adequate signal amplitude at low field but it is difficult to envisage a methodology that provides a systematic idealised polarisation state where the second spin system, in this case ^{1}H, is close to its equilibrium value for the relaxation field B_r. It should be possible with carefully manicured ^{1}H pulses and preparation periods but it would present a significant experimental challenge.

A field-cycling investigation is confronted with difficulties in multi-spin systems, however, as this example shows, if the preparation of the initial polarisations is systematic then all of the advantages of the field-cycling technique can be realised in providing accurate values for the correlation times and information on the mechanism driving the dynamics. This particular system benefited from relaxation processes that were dominated by the diagonal elements of the relaxation matrix, facilitating the analysis of the spectral density components and widths; the ^{13}C relaxation was often mono-exponential and the bi-exponential character was usually revealed only when the ^{1}H spin reservoir was far from equilibrium. In systems where the off-diagonal elements play a more significant role and bi-exponential behaviour is more apparent, as for example in ^{1}H–^{19}F heteronuclear systems [26], then alternative field-cycling methodologies must be adopted to determine all elements of the relaxation matrix individually. Only then can the relaxation data be reduced in such a way as to permit the spectral density components to be resolved with sufficient accuracy; such an investigation has been conducted on proton transfer in tetrafluoroterephthalic acid in our laboratory and will be the subject of a separate publication [32].

Acknowledgments

This work was supported by grants from the Royal Society (Paul Instrument Fund), the Engineering and Physical Sciences Research Council (EPSRC) and Bracco Imaging SpA.

References

[1] F. Noack, NMR field-cycling spectroscopy—principles and applications, Prog. Nucl. Magn. Reson. Spectrosc. 18 (1986) 171–276.
[2] R. Kimmich, E. Anoardo, Field-cycling NMR relaxometry, Prog. Nucl. Magn. Reson. Spectrosc. 44 (2004) 257–320.
[3] A.J. Horsewill, Q. Xue, Magnetic field-cycling investigations of molecular tunnelling, Phys. Chem. Chem. Phys. 4 (2002) 5475–5480.
[4] N. Bloembergen, E.M. Purcell, R.V. Pound, Relaxation effects in nuclear magnetic resonance absorption, Phys. Rev. 73 (1948) 679–712.
[5] B.H. Meier, F. Graf, R.R. Ernst, Structure and dynamics of intramolecular hydrogen bonds in carboxylic acid dimers—a solid state NMR study, J. Chem. Phys. 76 (1982) 767–774.
[6] E.R. Andrew, L. Latanowicz, Solid state proton transfer dynamics and the proton NMR 2nd moment and proton relaxation rates, J. Magn. Reson. 68 (1986) 232–239.
[7] A. Abragam, The Principles of Nuclear Magnetism, Clarendon Press, Oxford, 1961, p. 294.
[8] A. Stöckli, B.H. Meier, R. Kreis, R. Meyer, R.R. Ernst, Hydrogen bond dynamics in isotopically substituted benzoic acid dimers, J. Chem. Phys. 93 (1990) 1502–1520.
[9] J.L. Skinner, H.P. Trommsdorff, Proton transfer in benzoic acid crystals—A chemical spin boson problem—theoretical analysis of nuclear magnetic resonance, neutron scattering and optical experiments, J. Chem. Phys. 89 (1988) 897–907.
[10] D.F. Brougham, A.J. Horsewill, R.I. Jenkinson, Proton transfer dynamics in the hydrogen bonds: a direct measurement of the incoherent tunneling rate by NMR and the quantum-to-classical transition, Chem. Phys. Lett. 272 (1997) 69–74.
[11] A. Oppenländer, C. Rambaud, H.P. Trommsdorff, J.-C. Vial, Translational tunneling of protons in benzoic acid crystals, Phys. Rev. Lett. 63 (1989) 1432–1435.

[12] A.J. Horsewill, C.J. McGloin, H.P. Trommsdorff, M.R. Johnson, Proton tunneling in the hydrogen bonds of halogen-substituted derivatives of benzoic acid studied by NMR relaxometry: the case of large energy asymmetry, Chem. Phys. 291 (2003) 41–52.
[13] A. Heuer, U. Haeberlen, The dynamics of hydrogens in double well potentials—the transition of the jump rate from the low temperature quantum mechanical to the high temperature activated regime, J. Chem. Phys. 95 (1991) 4201–4212.
[14] M.A. Neumann, D.F. Brougham, C.J. McGloin, M.R. Johnson, A.J. Horsewill, H.P. Trommsdorff, Proton tunneling in benzoic acid crystals at intermediate temperatures: nuclear magnetic resonance and neutron scattering studies, J. Chem. Phys. 109 (1998) 7300–7311.
[15] Q. Xue, A.J. Horsewill, M.R. Johnson, H.P. Trommsdorff, Isotope effects associated with tunneling and double proton transfer in the hydrogen bonds of benzoic acid, J. Chem. Phys. 120 (2004) 11107–11119.
[16] W. Wu, D.L. Noble, A.J. Horsewill, The correspondence between quantum and classical mechanics: an experimental demonstration of the smooth transition between the two regimes, Chem. Phys. Lett. 402 (2005) 519–523.
[17] M. Plazanet, N. Fukushima, M.R. Johnson, A.J. Horsewill, H.P. Trommsdorff, The vibrational spectrum of crystalline benzoic acid: inelastic neutron scattering and density functional theory calculations, J. Chem. Phys. 115 (2001) 3241–3248.
[18] R.I. Jenkinson, A. Ikram, A.J. Horsewill, H.P. Trommsdorff, The quantum dynamics of proton transfer in benzoic acid measured by single crystal NMR spectroscopy and relaxometry, Chem. Phys. 294 (2003) 95–104.
[19] F. Fillaux, M.H. Limoge, F. Romain, Quantum proton transfer and interconversion in the benzoic acid crystal: vibrational spectra, mechanism and theory, Chem. Phys. 276 (2002) 181–210.
[20] C.C. Wilson, N. Shankland, A.J. Florence, A single crystal neutron diffraction study of the temperature dependence of hydrogen-atom disorder in benzoic acid dimers, J. Chem. Soc., Faraday Trans. 92 (1996) 5051–5057.
[21] D. Antoniou, S.D. Schwartz, Proton transfer in benzoic acid crystals: another look using quantum operator theory, J. Chem. Phys. 109 (1998) 2287–2293.
[22] S. Takeda, A. Tsuzumitani, An indication of slowing down of hydrogen atom transfer in isotopically mixed hydrogen bonds of benzoic acid crystals, Magn. Reson. Chem. 39 (2001) S44–S49.
[23] M.R. Johnson, H.P. Trommsdorff, Dispersion of vibrational modes in benzoic acid crystals, Chem. Phys. Lett. 364 (2002) 34–38.
[24] C.S. Tautermann, A.F. Voegele, K.R. Liedl, The ground-state tunneling splitting of various carboxylic acid dimers, J. Chem. Phys. 120 (2004) 631–637.
[25] P. Robyr, B.H. Meier, R.R. Ernst, Tensor correlation by 2D spin-diffusion powder NMR spectroscopy—determination of the asymmetry of the hydrogen bond potential in benzoic acid, Chem. Phys. Lett. 187 (1991) 471–478.
[26] A.J. Horsewill, A. Ikram, I.B.I. Tomsah, Hydrogen bond dynamics in tetrafluoroterephthalic acid studied by NMR and INS, Mol. Phys. 84 (1995) 1257–1272.
[27] A.J. Horsewill, I.B.I. Tomsah, Bi-exponential spin–lattice relaxation in solid hexfluoroactylacetone, Solid State Nucl. Magn. Reson. 2 (1993) 61–72.
[28] V.A. Benderskii, E.V. Vetoshkin, S.Yu. Grebenshchikov, L. von Laue, H.P. Trommsdorff, Tunneling splitting in vibrational spectra of non-rigid molecules. I. Perturbative instanton approach, Chem. Phys. 219 (1997) 119–142.
[29] V.A. Benderskii, E.V. Vetoshkin, L. von Laue, H.P. Trommsdorff, Tunneling splitting in vibrational spectra of non-rigid molecules. II. Excited states, Chem. Phys. 219 (1997) 143–160.
[30] V.A. Benderskii, E.V. Vetoshkin, H.P. Trommsdorff, Tunneling splittings in vibrational spectra of non-rigid molecules. X. Reaction path Hamiltonian as zero-order approximation, Chem. Phys. 271 (2001) 165–182.
[31] Z. Smedarchina, A. Fernandez-Ramos, W. Siebrand, Calculation of the tunnelling splitting in the zero-point level and CO-stretch fundamental of the formic acid dimer, Chem. Phys. Lett. 395 (2004) 339–345.
[32] W. Wu, A.J. Horsewill, Unpublished results.